

1 Citation: **Hirt, C.**, S.J. Claessens, T. Fecher, M. Kuhn, R. Pail, M. Rexer (2013), New ultra-high resolution picture of
2 Earth's gravity field, *Geophysical Research Letters*, Vol 40, doi: 10.1002/grl.50838.

3 4 **New ultra-high resolution picture of Earth's gravity field**

5
6 Christian Hirt^{1*}, Sten Claessens¹, Thomas Fecher², Michael Kuhn¹, Roland Pail², Moritz Rexer^{1,2}

7 ¹ Western Australian Centre for Geodesy, Curtin University, Perth, Australia

8 ² Institute for Astronomical and Physical Geodesy, Technical University Munich, Germany

9 * E-mail: c.hirt@curtin.edu.au

10 11 **Abstract**

12 We provide an unprecedented ultra-high resolution picture of Earth's gravity over all continents
13 and numerous islands within ± 60 degree latitude. This is achieved through augmentation of new
14 satellite and terrestrial gravity with topography data, and use of massive parallel computation
15 techniques, delivering local detail at ~ 200 m spatial resolution. As such, our work is the first-of-
16 its-kind to model gravity at unprecedented fine scales yet with near-global coverage. The new
17 picture of Earth's gravity encompasses a suite of gridded estimates of gravity accelerations,
18 radial and horizontal field components and quasigeoid heights at over 3 billion points covering
19 80% of Earth's land masses. We identify new candidate locations of extreme gravity signals,
20 suggesting that the CODATA standard for peak-to-peak variations in free-fall gravity is too low
21 by about 40%. The new models are beneficial for a wide range of scientific and engineering
22 applications and freely available to the public.

23 24 **Keywords**

25 Earth's gravity field, gravity, quasigeoid, vertical deflections, ultra-high resolution

26 27 **1 Introduction**

28
29 Precise knowledge of the Earth's gravity field structure with high resolution is essential for a
30 range of disciplines, as diverse as exploration and potential field geophysics [*Jakoby and Smilde,*
31 2009], climate and sea level change research [*Rummel, 2012*], surveying and engineering
32 [*Featherstone, 2008*] and inertial navigation [*Grejner-Brzezinska and Wang, 1998*]. While there
33 is a strong scientific interest to model Earth's gravity field with ever-increasing detail, the
34 resolution of today's gravity models remains limited to spatial scales of mostly 2-10 km globally
35 [*Pavlis et al., 2012; Balmino et al., 2012*], which is insufficient for local gravity field
36 applications such as modelling of water flow for hydro-engineering, inertial navigation or in-situ
37 reduction of geophysical gravity field surveys. Up until now, gravity models with sub-km
38 resolution are unavailable for large parts of our planet.

39
40 Here we provide an unprecedented ultra-high resolution view of five components of Earth's
41 gravity field over all continents, coastal zones and numerous islands within ± 60 degree latitude.
42 This is achieved through augmentation of new satellite and terrestrial gravity with topography
43 data [e.g., *Hirt et al. 2010*] and use of massive parallel computation techniques, delivering local
44 detail at 7.2 arc-seconds (~ 200 m in North-South direction) spatial resolution (Section 2). As
45 such, our work is the first-of-its-kind to model gravity at ultra-fine scales yet with near-global
46 coverage. The new picture of Earth's gravity encompasses a suite of gridded estimates of gravity

47 accelerations, radial and horizontal field components and quasigeoid heights at over 3 billion
48 points covering 80% of Earth's land masses and 99.7% of populated areas (Section 3, 4). This
49 considerably extends our current knowledge of the gravity field. The gridded estimates are
50 beneficial for a range of scientific and engineering applications (Section 5) and freely available
51 to the public. Electronic supplementary materials are available providing full detail on the
52 methods applied in this study.

53

54 **2 Data and Methods**

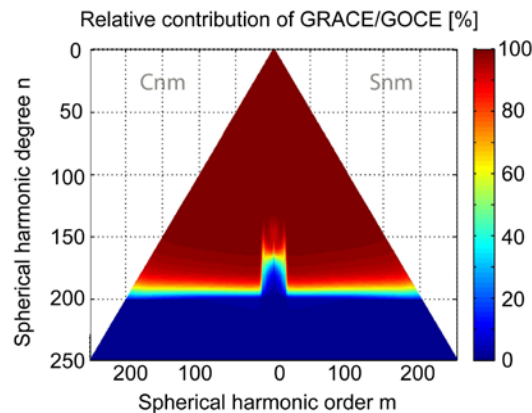
55

56 Our ultra-high resolution picture of Earth's gravity field is a combined solution based on the
57 three key constituents GOCE/GRACE satellite gravity (providing the spatial scales of ~10000
58 down to ~100 km), EGM2008 (~100 to ~10 km) and topographic gravity, i.e., the gravitational
59 effect implied by a high-pass filtered terrain model (scales of ~10 km to ~250 m),

60

61 Regarding the satellite component, we use the latest satellite-measured gravity data (release
62 GOCE-TIM4) from the European Space Agency's GOCE satellite [Drinkwater et al., 2003; Pail
63 et al., 2011], parameterized as coefficients of a spherical harmonic series expansion, that
64 currently provides the highest-resolution picture of Earth's gravity ever obtained from a space
65 gravity sensor. Resolving gravity field features at spatial scales as short as 80-100 km, GOCE
66 confers new gravity field knowledge, most notably over poorly surveyed regions of Africa,
67 South America and Asia [Pail et al., 2011].

68



69

70 **Figure 1.** Relative contribution of GOCE/GRACE data per spherical harmonic coefficient in the combination with
71 EGM2008 data (in percent) for the degrees 0 to 250

72

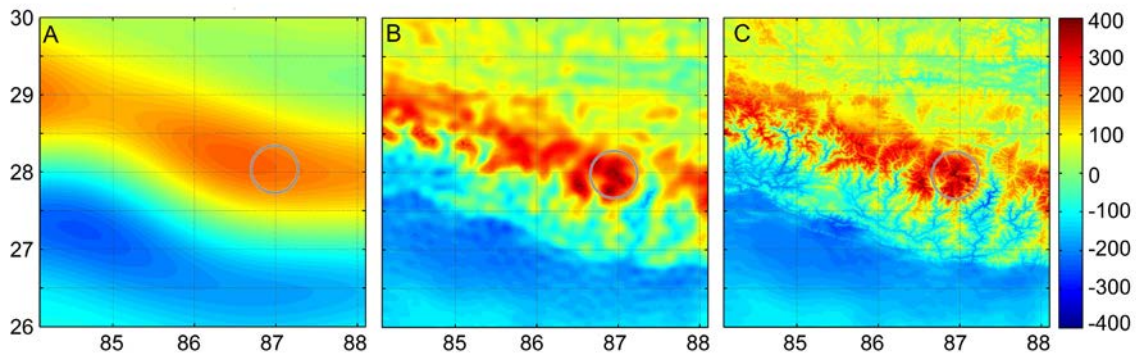
73 Compared to pure GOCE models, complementary GRACE satellite gravity [Mayer Guerr et al.,
74 2010] are superior in the spectral range up to degrees 70-80 [Pail et al., 2010]. Therefore, first a
75 combined satellite-only combined solution based on full normal equations of GRACE (up to
76 degree 180) and GOCE (up to degree 250) is computed [see, e.g., Pail et al., 2010]. The
77 GRACE/GOCE combination is then merged with EGM2008 [Pavlis et al., 2012] using the
78 EGM2008 coefficients as pseudo-observations. Since for EGM2008 only the error variances are
79 available, the corresponding normal equations have diagonal structure. In our combination,
80 GRACE/GOCE data have dominant influence in the spectral band of harmonic degrees 0 to 180
81 with EGM2008 information taking over in the spectral range 200 to 2190, leaving the main
82 spectral range of transition from GRACE/GOCE to EGM2008 in spectral band of degrees 181 to

83 200. The relative contributions of EGM2008 and GRACE/GOCE satellite gravity are shown in
84 Fig. 1.

85
86
87

88 The spherical-harmonic coefficients of the combined GRACE/GOCE/EGM2008 (GGE) gravity
89 model were used in the spectral band of degrees 2 to 2190 to synthesize a range of frequently
90 used gravity field functionals at the Earth's surface. For accurate spherical harmonic synthesis at
91 the Earth's surface, as represented through the SRTM topography, the gradient approach to fifth-
92 order [Hirt 2012] was applied. This numerically efficient evaluation technique takes into account
93 the effect of gravity attenuation with height. Applying the gradient approach as described in Hirt
94 [2012] yielded numerical estimates for radial derivatives (gravity disturbances) and horizontal
95 derivatives (deflections of the vertical) of the disturbing potential and quasigeoid heights from
96 the GGE data set at 7.2 arc-sec resolution (about 3 billion surface points) within the SRTM data
97 coverage.

98



99

100 **Figure 2.** Gravity field at different levels of resolution over Mount Everest area. A: satellite-only (free-air) gravity
101 from GOCE and GRACE satellites, B: GGE gravity (satellite gravity combined with EGM2008 gravity), C:
102 GGMplus as composite of satellite gravity, EGM2008 and topographic gravity. Shown is the radial component of
103 the gravity field over a $\sim 400 \times 400$ km area covering parts of the Southern Himalayas including the Mount Everest
104 summit area (marked), units in 10^{-5} m s^{-2} . The spatial resolution of the gravity modelling increases from ~ 100 km
105 (A), ~ 10 km (B) to ultra-fine ~ 200 m spatial scales (C).

106

107 For the Mount Everest region, Fig. 2 exemplifies the associated resolution of GOCE/GRACE
108 satellite gravity (A) and their combination with EGM2008 gravity (B). The spatial resolution of
109 the GGE gravity field functionals is limited to about ~ 10 km (or harmonic degree of 2190) which
110 leaves the problem of modelling the field structures at short scales, down to few 100 m
111 resolution at any of the surface points.

112

113 Because ground gravity measurements at a spatial density commensurate with our model
114 resolution do not exist over most parts of Earth [e.g., Sansò and Sideris, 2013] – and will not
115 become available in the foreseeable future – alternative solutions are required to estimate the
116 gravity field signals at scales shorter than 10 km. High-resolution topography data is widely
117 considered the key to ultra-high resolution gravity modelling and used successfully as effective
118 means to estimate short-scale gravity effects [Sansò and Sideris, 2013; Tziavos and Sideris,
119 2013, Pavlis et al., 2012; Forsberg and Tscherning, 1981]. This is because the short-scale
120 gravity field is dominated by the constituents generated by the visible topographic masses

121 [Forsberg and Tscherning, 1981]. However, forward estimation of the short-scale gravity field
 122 constituents from elevation models near-globally at ultra-high (few 100 metres) resolution is
 123 computationally demanding. Yet we have accomplished this challenge for the first time through
 124 advanced computational resources.

125
 126 Massive parallelization and the use of Western Australia’s iVEC/Epic supercomputing facility
 127 allowed us to convert topography from the Shuttle Radar Topography Mission (SRTM), cf.
 128 Jarvis et al. [2008] – along with bathymetric information along coastlines [Becker et al., 2009] –
 129 to topographic gravity at 7.2 arc-sec resolution everywhere on Earth between $\pm 60^\circ$ latitude with
 130 SRTM data available. Based on non-parallelized standard computation techniques, the
 131 calculation of topographic gravity effects would have taken an estimated 20 years, which is why
 132 previous efforts were restricted to regional areas [Kuhn et al., 2009; Hirt, 2012].

133
 134 The conversion of topography to topographic gravity is based on the residual terrain modelling
 135 technique [Forsberg, 1984], with the topography high-pass filtered through subtraction of a
 136 spherical harmonic reference surface (of degree and order 2160) prior to the forward-modelling.
 137 We treated the ocean water masses and those of the major inland water bodies (Great Lakes,
 138 Baikal, Caspian Sea) using a combination of residual terrain modelling with the concept of rock-
 139 equivalent topography [Hirt, 2013], whereby the water masses were ‘compressed’ to layers
 140 equivalent to topographic rock. These procedures yield short-scale topographic gravity that is
 141 suitable for augmentation of degree-2190 spherical harmonic gravity models beyond their
 142 associated 10 km resolution, cf. Hirt [2010; 2013]. The topographic gravity is based on a mass-
 143 density assumption of 2670 kg m^{-3} and provides the spatial scales of $\sim 10 \text{ km}$ to $\sim 250 \text{ m}$, which is
 144 complementary to the GGE gravity (spatial scales from $\sim 10000 \text{ km}$ to $\sim 10 \text{ km}$).

145
 146 **3 Results**

147
 148 Addition of both components (GGE and topographic gravity) result in the ultra-high resolution
 149 model GGMplus (Global Gravity Model, with plus indicating the leap in resolution over
 150 previous 10 km resolution global gravity models). The modelled gravity field components and
 151 their descriptive statistics are reported in Table 1.

152
 153 **Table 1.** Descriptive statistics of the GGMplus model components calculated at 3,062,677,383 land and
 154 near-coastal points within $\pm 60^\circ$ geographic latitude. RMS is the root-mean-square of the component.

Gravity model component		Min	Max	RMS	Unit
Gravity	Free-fall acceleration	976392	981974	980133	10^{-5} m s^{-2}
	Radial component	-456	714	48.0	10^{-5} m s^{-2}
Horizontal components	North-South	-108	94	6.9	arc-sec
	East-West	-83	79	6.8	arc-sec
	Total (magnitude)	0	109	9.4	arc-sec
Quasigeoid		-99.26	86.60	29.91	m

155
 156 This world-first ultra-high resolution modelling over most of Earth’s land areas delivered us the
 157 expected gravity signatures of small-scale topographic features – such as mountain peaks and
 158 valleys – which are otherwise masked in 10 km resolution models. This adds much local detail to
 159 the gravity maps (compare Figs. 2B and 2C) and yields a spectrally more complete and accurate
 160 description of the gravity field [e.g., Hirt, 2012].

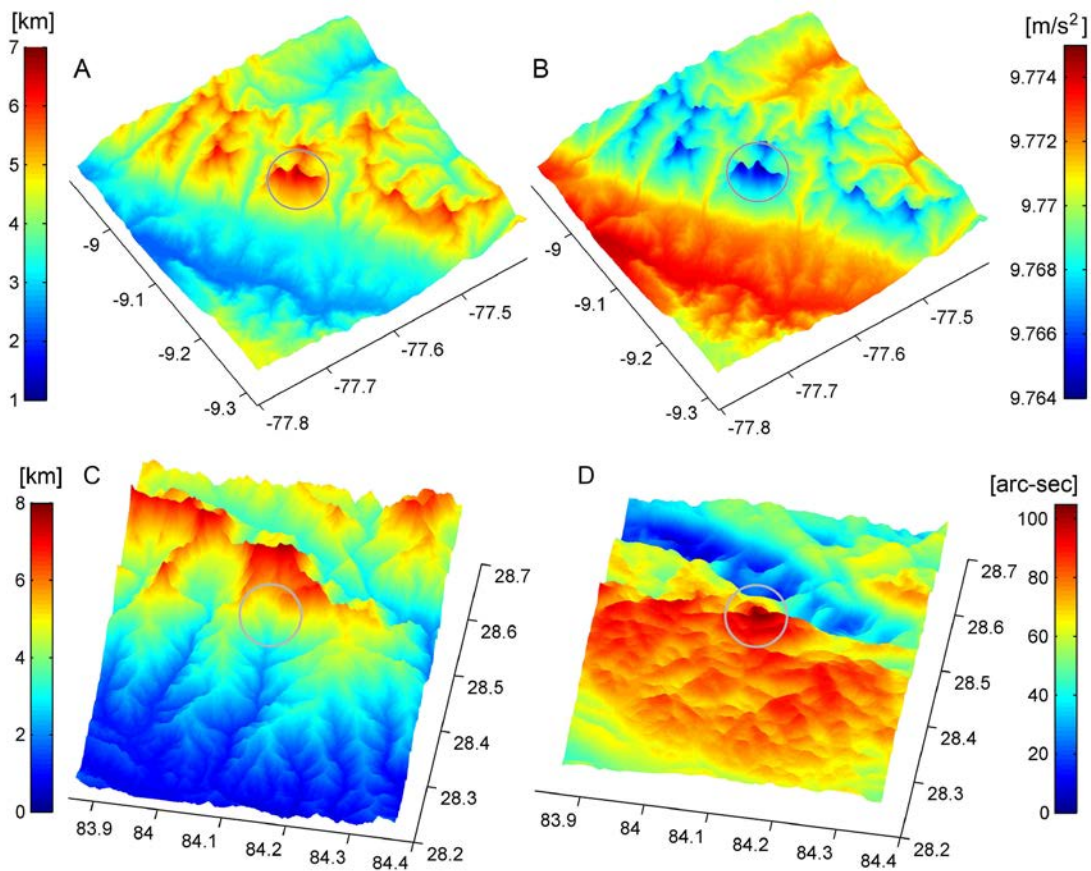
161 **Table 2.** Candidate locations for extreme values of Earth's gravity field

Gravity component	Minimum/ Maximum	Latitude/ Longitude	Geographic feature/ location
Gravity acceleration	9.76392 m s ⁻² 9.83366 m s ⁻²	-9.12°/ -77.60° 86.71°/61.29°	Huascarán, Peru *Arctic Sea
Radial component	-456 × 10 ⁻⁵ m s ⁻² 714 × 10 ⁻⁵ m s ⁻²	29.71°/95.36° 10.83°/-73.69°	Gandengxiang, China Pico Cristóbal Colón, Columbia
Horizontal component ⁺	109 arc-sec	28.45°/84.13°	~10 km South of Annapurna II, Nepal
Quasigeoid	-106.59 m 86.60 m	4.71°/78.79° -8.40°/147.35°	*Laccadive Sea, South of Sri Lanka Puncak Trikora, Papua, Indonesia

162 * offshore area, value estimated without topographic gravity using GGE-only (10 km resolution, also see
163 electronic supplement)

164 ⁺ total component computed as magnitude from the North-South and East-West components

165



166 **Figure 3.** Candidate locations of some extreme signals in Earth's gravity in the Andes (A,B) and Himalaya regions
167 (C,D). Top: Topography (A) and free-fall gravity accelerations (B) over the Huascarán region (Peru), where
168 GGMplus gravity accelerations are as small as ~9.764 m s⁻² (B). Bottom: Topography (C) and GGMplus total
169 horizontal field component (D) over the Annapurna II region (Nepal). The gravitational attraction of the Annapurna
170 II masses is expected to cause an extreme slope of the quasi/geoid with respect to the Earth ellipsoid of up to ~109
171 arc-seconds (D).
172

173 Our gridded estimates portray the subtle variations of gravity (Fig. 3) which are known to depend
174 on factors such as location, height and presence of mass-density anomalies. GGMplus reveals a
175 candidate location for the minimum gravity acceleration on Earth: the Nevado Huascarán summit
176 (Peru) with an estimated acceleration of 9.76392 m s^{-2} (Fig 3A, 3B, and Table 2). A candidate
177 location for Earth's maximum gravity acceleration was identified - outside the SRTM area, based
178 on GGE-only – in the Arctic sea with an estimated 9.83366 m s^{-2} . This suggests a variation range
179 (peak-to-peak variation) for gravity accelerations on Earth of about $\sim 0.07 \text{ m s}^{-2}$, or 0.7 %, which
180 is about 40 % larger than the variation range of 0.5 % implied by standard models based on a
181 rotating mass-ellipsoid (gravity accelerations are 9.7803 m s^{-2} (equator) 9.8322 m s^{-2} (poles) on
182 the mass-ellipsoid, cf. *Moritz* [2000]). So far such a simplified model is also used by the
183 Committee on Data for Science and Technology (CODATA) to estimate the variation range in
184 free-fall acceleration on Earth [*Mohr and Taylor*, 2005]. However, due to the inhomogeneous
185 structure of Earth, presence of topographic masses, and decay of gravity with height the actual
186 variations in free-fall accelerations are $\sim 40\%$ larger at the Earth's surface (Table 2).

187
188 GGMplus free-air gravity – the radial component of Earth's gravity field – varies within a range
189 of $\sim 0.011 \text{ m s}^{-2}$ ($\sim 0.1\%$ of gravity accelerations) with its minimum value of $-456 \times 10^{-5} \text{ m s}^{-2}$
190 located in China and its maximum of $714 \times 10^{-5} \text{ m s}^{-2}$ expected for the Pico Cristóbal Colón
191 summit in Colombia. The higher variability of gravity accelerations over free-air gravity reflects
192 the well-known fact that gravity accelerations include the gravitational attraction and centrifugal
193 effect due to Earth rotation.

194
195 The horizontal components of the gravitational field describe in approximation the North-South
196 and East-West inclination of the quasi/geoid with respect to the reference ellipsoid. The variation
197 range of the horizontal field components (also known as deflections of the vertical) is about ~ 200
198 arc-seconds in North South, and ~ 160 arc-seconds in East-West, respectively (Table 1).
199 GGMplus reveals a candidate location for Earth's largest deflection of the vertical: about 10 km
200 South of Annapurna II, Nepal, the plumb line is expected to deviate from the ellipsoid normal by
201 an angle as large as ~ 109 arc-seconds (Fig. 3C and 3D). This translates into a most extreme
202 quasi/geoid slope of about 0.5 m over 1 km.

203 204 **4 Model evaluation**

205
206 We have comprehensively compared GGMplus gravity field maps with in-situ (direct)
207 observations of Earth's gravity field from gravimetry, astronomy, and surveying (see electronic
208 supplementary materials). Over well-surveyed areas of North America, Europe and Australia,
209 the comparisons suggest an accuracy level for free-air gravity and gravity accelerations of $\sim 5 \times$
210 10^{-5} m s^{-2} , for horizontal field components of about 1 arc-second, and for quasigeoid heights of
211 0.1 m or better.

212
213 Despite the improvements conferred by recent satellite gravity to our model, the GGMplus
214 accuracy deteriorates by a factor of ~ 3 to ~ 5 over Asia, Africa and South America which are
215 regions with limited or very limited ground gravity data availability. Comparisons suggest a
216 decrease in accuracy down to $\sim 20 \times 10^{-5} \text{ m s}^{-2}$ for gravity, ~ 5 arc-seconds for horizontal field
217 components, and ~ 0.3 m for quasigeoid heights. The reduced accuracy estimates mainly reflect
218 the limited availability of gravity observations at spatial scales of ~ 100 to ~ 10 km. The accuracy

219 of GGMplus gravity accelerations will always be lower than that of free-air gravity. This is
220 because accelerations are directly affected by errors in the elevation data, with an elevation error
221 of 10 m equivalent to about $3 \times 10^{-5} \text{ m s}^{-2}$.

222
223 Given that any gravity field signals originating from local mass-density variations are not
224 represented by the topographic gravity, our gravity maps cannot provide information on
225 geological units at scales less than 10 km. This is akin to EGM2008 at spatial scales of ~30 to
226 ~10 km over many land areas where gravity measurements are unavailable or of proprietary
227 nature [Pavlis *et al.*, 2012]. Any global, regional or local gravity map or quasi/geoid model can
228 only be geologically interpreted down to a resolution commensurate with the gravity
229 observations used to construct the model. Nevertheless, incorporation of topographic gravity to
230 approximate gravity field features at spatial scales of ~10 km to ~250 m significantly improves
231 GGMplus gravity and horizontal components when compared to 10 km-resolution maps.
232 Depending on the terrain ruggedness, the observed improvement rates mostly range between 40
233 to 90% for radial and horizontal field components (Supplementary Tables 6 and 8), while the
234 quasigeoid improvement is best observable over rugged areas (up to 40 % improvement,
235 Supplementary Table 9).

236
237 **5 Applications**
238 Apart from enhancing our knowledge of Earth's gravity and its variations, there are several
239 scientific and engineering applications that require high-resolution and largely complete gravity
240 knowledge, which is now available through GGMplus gravity maps.

241
242 The quasi/geoid plays a crucial role in modern determination of topographic heights with Global
243 Navigation Satellite Systems (such as the Global Positioning System GPS), allowing the
244 measurement of heights above mean sea level rather than heights above the ellipsoid [e.g., Meyer
245 *et al.*, 2006; Featherstone, 2008; Hirt *et al.*, 2011]. While several regional-size quasi/geoid
246 models of good quality are available at mostly ~2 km resolution over well-surveyed land areas
247 (e.g., Europe, USA, Australia), GGMplus is capable of providing improved quasi/geoid
248 information over those parts of Asia, Africa and South America, where no other source of high-
249 resolution gravity (e.g., from airborne gravity) is available. The GGMplus quasigeoid can be
250 suitable for water flow modelling (e.g., as required in hydro-engineering), and height transfer
251 with satellite systems, and can be of utility for the determination of offsets among continental
252 height systems (e.g., Australia and Europe) and their unification [e.g., Flury and Rummel, 2005;
253 Rummel, 2012]. This in turn will allow for a more consistent comparison of sea level
254 observations at tide gauges across the oceans. Because of incorporation of newer GOCE and
255 GRACE satellite gravity, the GGMplus quasigeoid confers improvements at ~100 km spatial
256 scales over parts of Asia, South America and Africa, while consideration of short-scale
257 quasigeoid effects from topography data improves the resolution of quasigeoid heights over
258 rugged terrain [Hirt *et al.*, 2010].

259
260 GGMplus gravity accelerations and free-air gravity are a promising data source for screening and
261 outlier-detection of terrestrial gravity databases and aid in planning of local precision gravimetric
262 surveys. Gravity accelerations as provided by our maps are required e.g., as a correction in the
263 context of geodetic height systems [e.g., Meyer *et al.*, 2006], for accurate topographic mapping,
264 in metrology for calibration of precision scales [Torge, 1989] and seismometers, and in

265 observational astronomy for meteorological corrections [Corbard *et al.*, 2013]. For geophysics
266 and the exploration industry, GGMplus may prove beneficial as novel data source for in-situ
267 reduction of detailed gravimetric surveys, revealing locations of interest for mineral prospectivity
268 without the need to calculate and apply further rather time-consuming reductions [Jakoby and
269 Smilde, 2009] Finally, horizontal field components are required to correct the impact of the
270 Earth's irregular gravity field, e.g., for inertial navigation at or near the Earth's surface [Grejner-
271 Brzezinska and Wang, 1998], or in the context of civil engineering (e.g., precision surveys for
272 tunnel alignment), Featherstone and Rieger [2000]. All of these applications require spectrally
273 most complete information on the gravity field.

274

275 **6 Conclusions**

276

277 GGMplus provides the most complete description of Earth's gravity at ultra-high resolution and
278 near-global coverage to date. This confers immediate benefits to many applications in
279 engineering, exploration, astronomy, surveying, and potential field geophysics. While GGMplus
280 provides moderate additional information (because of the ultra-high resolution short-scale
281 modelling) over areas with dense coverage of gravity stations (e.g., North America, Europe,
282 Australia), significant improvements are provided over areas with sparse ground gravity
283 coverage (e.g., Asia, Africa, South America). For the latter regions, GGMplus provides for the
284 first time a complete coverage with gravity at ultra-high spatial resolution, thus providing
285 scientific aid to many developing countries. In addition, GGMplus provides crucial information
286 to revise current standards for the maximum range of free-fall gravity accelerations over the
287 Earth's surface. The computerized GGMplus gravity field maps are freely available for science,
288 education and industry via [and http://ddfe.curtin.edu.au/gravitymodels/GGMplus](http://ddfe.curtin.edu.au/gravitymodels/GGMplus).

289

290 **Acknowledgements** We are grateful to the Australian Research Council for funding
291 (DP120102441). This work was made feasible through using advanced computational resources
292 of the iVEC/Epic supercomputing facility (Perth, Western Australia). We thank all developers
293 and providers of data used in this study. Full methods, and detailed evaluation results are
294 available in the electronic supplementary information, and information on data access via the
295 project's website <http://geodesy.curtin.edu.au/research/models/GGMplus>.

296

297 **References**

- 298 Balmino, G., N. Vales, S. Bonvalot and A. Briais (2012), Spherical harmonic modelling to ultra-high degree of
299 Bouguer and isostatic anomalies, *J. Geod.*, 86(7), 499-520, doi: 10.1007/s00190-011-0533-4.
- 300 Becker, J.J., D.T. Sandwell, W.H.F. Smith, J. Braud, B. Binder, J. Depner, D. Fabre, J. Factor, S. Ingalls, S-H. Kim,
301 R. Ladner, K. Marks, S. Nelson, A. Pharaoh, R. Trimmer, J. Von Rosenberg, G. Wallace and P. Weatherall
302 (2009), Global Bathymetry and Elevation Data at 30 Arc Seconds Resolution: SRTM30_PLUS, *Marine*
303 *Geod.*, 32(4), 355-371.
- 304 Corbard T., F. Morand, F. Laclarex, R. Ikhlef, and M. Meftah (2013), On the importance of astronomical refraction
305 for modern Solar astrometric measurements, *Astr. Astrophys.*, April 2, 2013.
- 306 Drinkwater, M.R., R. Floberghagen, R. Haagmans, D. Muzi, and A. Popescu (2003), GOCE: ESA's first Earth
307 Explorer Core mission, In (eds. Beutler, G.B., M.R. Drinkwater, R. Rummel, and R. von Steiger), Earth
308 Gravity Field from Space - from Sensors to Earth Sciences. In the Space Sciences Series of ISSI, Vol. 18,
309 419-432, *Kluwer Academic Publishers*, Dordrecht, Netherlands ISBN: 1-4020-1408-2.
- 310 Featherstone W.E. (2008), GNSS-based heighting in Australia: current, emerging and future issues, *J. Spat. Sci.* 53,
311 115-133.
- 312 Featherstone W.E., and J.M. Rieger (2000), The importance of using deviations of the vertical for the reduction of
313 survey data to a geocentric datum, *Australian Surveyor*, 45, 46-61.

314 Flury, J., and R. Rummel (2006), Future satellite gravimetry for geodesy, *Earth Moon Plan.* 94, 13-29.
315 doi:10.1007/s11038-005-3756-7

316 Forsberg R., and C.C. Tscherning (1981), The use of height data in gravity field approximation by collocation, *J.*
317 *Geophys. Res.*, 86(B9), 7843-7854.

318 Forsberg, R. (1984), A study of terrain reductions, density anomalies and geophysical inversion methods in gravity
319 field modelling, Report 355, *Department of Geodetic Science and Surveying*, Ohio State University,
320 Columbus.

321 Grejner-Brzezinska, D.A., and J. Wang (1998), Gravity modeling for high-accuracy GPS/INS integration,
322 *Navigation*, 45, 3, 209-220.

323 Hirt, C. (2010), Prediction of vertical deflections from high-degree spherical harmonic synthesis and residual terrain
324 model data, *J. Geod.*, 84 (3), 179-190. doi:10.1007/s00190-009-0354-x

325 Hirt, C., W.E. Featherstone and U. Marti (2010), Combining EGM2008 and SRTM/DTM2006.0 residual terrain
326 model data to improve quasigeoid computations in mountainous areas devoid of gravity data, *J. Geod.*, 84(9):
327 557-567, DOI: 10.1007/s00190-010-0395-1..

328 Hirt C., Schmitz M., Feldmann-Westendorff U., Wübbena G., Jahn C.-H., and Seeber G. (2011), Mutual validation
329 of GNSS height measurements from high-precision geometric-astronomical levelling, *GPS Solutions*, 15(2),
330 149-159, DOI 10.1007/s10291-010-0179-3.

331 Hirt, C. (2012), Efficient and accurate high-degree spherical harmonic synthesis of gravity field functionals at the
332 Earth's surface using the gradient approach, *J. Geod.*, 86(9), 729-744, doi: 10.1007/s00190-012-0550-y.

333 Hirt, C. (2013), RTM gravity forward-modeling using topography/bathymetry data to improve high-degree global
334 geopotential models in the coastal zone, *Marine Geod.*, 36(2):1-20, doi:10.1080/01490419.2013.779334.

335 Jacoby, W., and P.L. Smilde (2009), *Gravity interpretation*, Springer, Berlin, Heidelberg.

336 Jarvis, A., H.I. Reuter, A. Nelson, and E. Guevara (2008), Hole-filled SRTM for the globe Version 4, *Available from*
337 *the CGIAR-SXI SRTM 90m database*. Available at: <http://srtm.csi.cgiar.org>.

338 Kuhn, M., W.E. Featherstone, and J.F. Kirby (2009), Complete spherical Bouguer gravity anomalies over Australia,
339 *Australian J. Earth Sci.*, 56, 213-223.

340 Mohr P. J., and B.N. Taylor (2005), CODATA recommended values of the fundamental physical constants: 2002,
341 *Rev. Mod. Phys.* 77 (Jan 2005).

342 Moritz, H. (2000), Geodetic Reference System 1980. *J. Geod.*, 74, 128-140.

343 Meyer T.H., D.R. Roman, and D.B. Zilkoski (2006), What Does Height Really Mean? Part IV: GPS Heighting.
344 *Surveying Land Inf. Sci.* 66, 165-183.

345 Mayer-Gürr, T., E. Kurtenbach, and A. Eicker (2010), ITG-Grace2010 Gravity Field Model. URL:
346 <http://www.igg.uni-bonn.de/apmg/index.php?id=itg-grace2010>, 2010.

347 Pail, R., Goiginger, H., W.-D. Schuh, E. Höck, J.M. Brockmann, T. Fecher, T. Gruber, T. Mayer-Gürr, J. Kusche, A.
348 Jäggi, and D. Rieser (2010), Combined satellite gravity field model GOCO01S derived from GOCE and
349 GRACE, *Geophys. Res. Lett.* 37, L20314, doi: 10.1029/2010GL044906.

350 Pail, R., S. Bruinsma, F. Migliaccio, C. Förste, H. Goiginger, W.-D. Schuh, E. Höck, M. Reguzzoni, J.M.
351 Brockmann, O. Abrikosov, M. Veicherts, T. Fecher, R. Mayrhofer, I. Krasbutter, F. Sansò, and C.C.
352 Tscherning (2011), First GOCE gravity field models derived by three different approaches, *J Geod.*, 85(11),
353 819-843, doi: 10.1007/s00190-011-0467-x.

354 Pavlis N.K., S.A. Holmes, S.C. Kenyon, and J.K. Factor (2012), The development and evaluation of the Earth
355 Gravitational Model 2008 (EGM2008), *J. Geophys. Res.*, 117, B04406, doi:10.1029/2011JB008916.

356 Rummel, R. (2012), Height unification using GOCE. *J. Geod. Sci.* 2, 355-362.

357 Sansò F., and M.G. Sideris (2013), The Local Modelling of the Gravity Field: The Terrain Effects. *Lecture Notes in*
358 *Earth System Sciences* 110, 169, Springer, Berlin Heidelberg.

359 Tziavos, I.N., and M.G. Sideris (2013), Topographic Reductions in Gravity and Geoid Modeling. *Lecture Notes in*
360 *Earth System Sciences* 110, 337-400, Springer, Berlin Heidelberg.

361 Torge W. (1989), *Gravimetry*, de Gruyter, Berlin, New York.

362
363
364
365
366
367
368
369

New ultra-high resolution picture of Earth's gravity field

Christian Hirt^{1*}, Sten Claessens¹, Thomas Fecher², Michael Kuhn¹, Roland Pail², Moritz Rexer^{1,2}

¹ Western Australian Centre for Geodesy, Curtin University, Perth, Australia

² Institute for Astronomical and Physical Geodesy, Technical University Munich, Germany

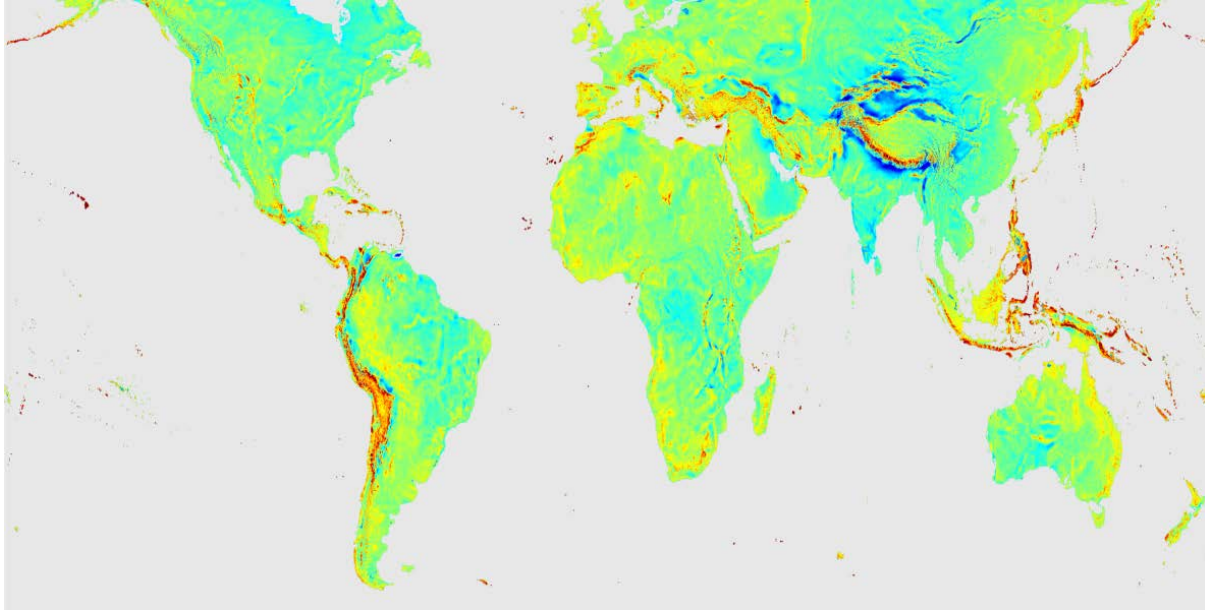
1 General

The development of GGMplus was driven by our vision to provide for the first time widely complete gravity field knowledge on a near-global scale to users of the scientific and engineering community as well as for education purposes based on freely-available data sources.

The model development was facilitated by the availability of new satellite observations of Earth's gravity field, as well as detailed topographic elevation data (Sect. 2), availability of suitable and efficient methods for highest-resolution gravity modelling (Sect. 3) and, importantly, made possible through advanced supercomputing resources provided by the iVEC/Epic supercomputing centre of Western Australia.

Coverage

GGMplus provides computerized gravity field maps at 7.2 arc-seconds (0.002° or ~224 m in latitude direction) resolution for all land areas of Earth within $\pm 60^\circ$ geographic latitude (as represented by SRTM, with the exception of the Southern part of Greenland), and an adjoining ~10 km marine zone along the coast lines (Fig. 1). The target resolution of GGMplus of 7.2 arc-seconds translates into a total of ~3 billion computation points within our working area. The chosen resolution allows representing the short-scale variations of the radial (gravity) and horizontal field components (deflections of the vertical).



401 **Figure 1.** Coverage of GGMplus. Shown are mean values of the radial component of the gravity
 402 field over land and near-coastal areas between $\pm 60^\circ$ geographic latitude.
 403

404
 405 *Technical definitions*

406
 407 The five gravity field functionals provided by GGMplus are
 408

- 409 • Free-fall gravity accelerations (i.e. gravitational plus centrifugal accelerations)
- 410 • Gravity disturbances (radial derivatives of the disturbing potential), denoted as radial
 411 component of the gravity field in the manuscript
- 412 • North-South deflection of the vertical in Helmert definition (latitudinal derivative of the
 413 disturbing potential), denoted as horizontal component of the gravity field in the
 414 manuscript
- 415 • East-West deflection of the vertical in Helmert definition (longitudinal derivative of the
 416 disturbing potential), denoted as horizontal component of the gravity field in the
 417 manuscript
- 418 • and Molodenski quasigeoid heights.

419
 420 All quantities are given at the Earth’s surface as defined through the SRTM (Shuttle Radar
 421 Topography Mission) topography. Users wishing to use geoid heights instead of quasigeoid
 422 heights can do so by applying standard conversion as described, e.g., *Rapp* [1997].
 423

424 **2 Data sets used**

425
 426 A complete list of data sets used for the development of GGMplus is given in Table 1. The use of
 427 these data is further detailed in Section 3.
 428

429 Table 1. Data sets used for the development of GGMplus

Dataset	Resource	Citation
---------	----------	----------

GRACE satellite gravity model ITG2010s	http://icgem.gfz-potsdam.de/ICGEM	<i>Mayer-Gürr et al.</i> [2010]
GOCE-TIM4 satellite gravity model	http://icgem.gfz-potsdam.de/ICGEM/	<i>Pail et al.</i> , [2011]
EGM2008 gravity model	http://earth-info.nga.mil/GandG/wgs84/gravitymod/egm2008/	<i>Pavlis et al.</i> , [2012]
Gridded 250 m SRTM V4.1 release over land	http://srtm.csi.cgiar.org/	<i>Jarvis et al.</i> , [2008]
Gridded SRTM30_PLUS V7 bathymetry offshore	http://topex.ucsd.edu/WWW_html/srtm30_plus.html	<i>Becker et al.</i> , [2009]
RET2012 spherical harmonic rock-equivalent topography model	http://www.geodesy.curtin.edu.au/research/models , file Earth2012.RET2012.SHcto2160.zip	<i>Hirt et al.</i> , [2012]
Earth2012 Topo/Air spherical harmonic model of Earth's physical surface	http://www.geodesy.curtin.edu.au/research/models , file Earth2012.topo_air.SHcto2160.zip	<i>Hirt et al.</i> , [2012]

430

3 Methods

431

432

433 GGMplus is constructed as a composite model of GOCE and GRACE satellite gravity,
 434 EGM2008 and topographic gravity in the space domain. The following steps were taken to
 435 develop the model:

- 436 • Combination of GOCE and GRACE satellite gravity (Sect. 3.1)
- 437 • Combination of GOCE-GRACE combined model with EGM2008 (Sect. 3.2)
- 438 • Spherical harmonic synthesis of gravity field quantities (Sect. 3.3)
- 439 • Forward-modelling of gravity field quantities (Sect. 3.4)
- 440 • Calculation of normal gravity at the Earth's surface (Sect. 3.5)
- 441 • Combination of synthesis and forward-modelling results (Sect. 3.6)

442

443 The 250 m resolution SRTM topography [*Jarvis et al.*, 2008] is consistently used to represent
 444 Earth's physical surface in the gravity field synthesis (Sect. 3.3), forward-modelling (Sect. 3.4)
 445 and calculation of normal gravity (Sect. 3.4). In approximation, SRTM elevations are physical
 446 heights above mean sea level. In processing steps 3.3 and 3.5, heights of the topography above
 447 the ellipsoid (ellipsoidal heights) are required. These were obtained in approximation as sum of
 448 SRTM and the EGM2008 quasigeoid [*Pavlis et al.*, 2012]. The geoid-quasigeoid separation was
 449 not accounted for in the construction of SRTM ellipsoidal heights, because this effect is mostly
 450 small (cm-dm-level, up to 1-2 m in the high mountains), which play a negligible role in 3D
 451 spherical harmonic synthesis. The parameters of the GRS80 geodetic reference system [*Moritz*,
 452 2000] were consistently used throughout the GGMplus model development.

453

454 3.1 *GOCE TIM4 and GRACE combination*

455

456 The satellite-only combination model has been computed by addition of full normal equations of
 457 GRACE and GOCE.

458

459

$$\begin{aligned}
 & \left[\sum_{i=1}^4 (A^T \Sigma(l)^{-1} A)_{GOCE,i} + A^T \Sigma(l)^{-1} A \right]_{GRACE} x = \\
 & \left[\sum_{i=1}^4 (A^T \Sigma(l)^{-1} l)_{GOCE,i} + A^T \Sigma(l)^{-1} l \right]_{GRACE} \Leftrightarrow N_{sat} x = n_{sat}
 \end{aligned} \tag{1}$$

461

462

463 The GRACE component consists of ITG-Grace2010s [Mayer-Gürr *et al.*, 2010] up to
 464 degree/order 180, which is based on GRACE K-band range rate and kinematic orbit data
 465 covering the time span from August 2002 to August 2009. The GOCE component contains
 466 reprocessed satellite gravity gradiometry data (main diagonal components V_{XX} , V_{YY} and V_{ZZ} and
 467 off-diagonal component V_{XZ} of the gravity gradient tensor; summation $i = 1, \dots, 4$ in Eq. (1)) from
 468 November 2009 to June 2012, as they have also been used for the 4th release of the GOCE TIM
 469 model [Pail *et al.*, 2011]. In Eq. (1), l are the observations, and x the unknown spherical
 470 harmonic coefficients (SHC).

471

472 In the frame of the gravity gradient reprocessing, among others an improved algorithm for
 473 angular rate reconstruction has been applied [Stummer *et al.*, 2011], leading to a significant
 474 improvement of the gravity gradient performance mainly in the low to medium degrees [Pail *et*
 475 *al.*, 2013]. The resulting GOCE gradiometry normal equations are resolved up to degree/order
 476 250.

477

478 Special emphasis has been given to realistic stochastic modeling of observation errors as part of
 479 the assembling and solution of the individual normal equation systems, yielding realistic
 480 variance-covariance information $\Sigma(l)$ for both GRACE and GOCE. In the case of GOCE, digital
 481 auto-regressive moving average (ARMA) filters have been used to set-up the variance-
 482 covariance information of the gradient observations [Pail *et al.*, 2011]. Technically, this is done
 483 by applying these filters to the full observation equation, i.e., both to the observations and the
 484 columns of the Jacobian (design matrix A). Due to the realistic stochastic modeling, the two
 485 normal equations could be combined with unit weight. Because of the further combination with
 486 EGM2008 as described in section 3.2, regularization has not been applied.

487

488 3.2 *GOCE/GRACE and EGM2008 combination*

489

490 The combination of the GRACE/GOCE data with EGM2008 is done on the basis of the
 491 combined GRACE/GOCE normal equations (see Sect. 3.1). Here the EGM2008 SHCs are
 492 treated as a set of *a priori* known parameters introduced into a least-squares process of the form:

493

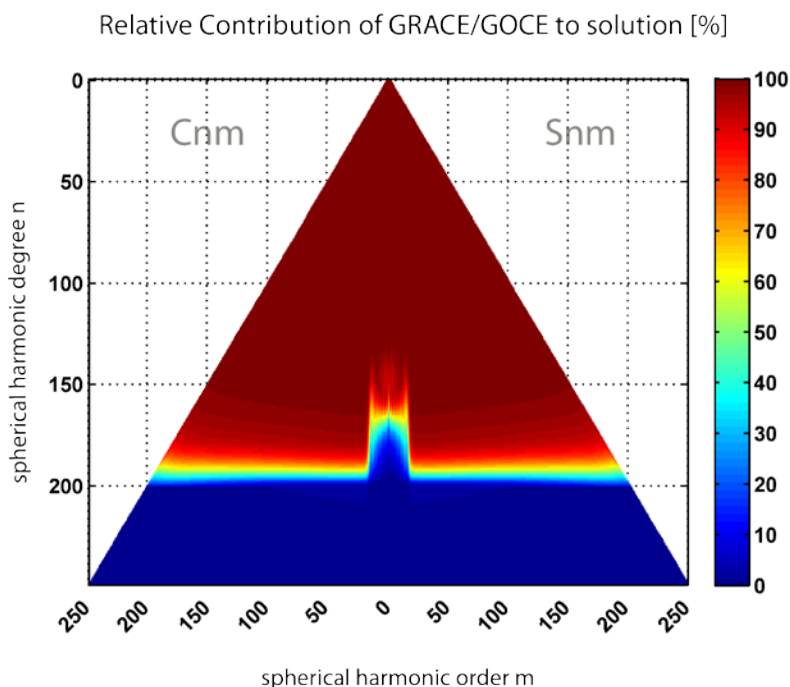
$$(w_1 N_{sat} + w_2 \Sigma(x_{EGM})^{-1}) x = w_1 n_{sat} + w_2 \Sigma(x_{EGM})^{-1} x_{EGM} \tag{2}$$

495

496 where x is the optimally combined set of SHCs from GRACE, GOCE and EGM2008. The
 497 terms N_{sat} and n_{sat} denote the normal equation system of GRACE/GOCE combination (cf.
 498 section 3.1), resolved up to degree/order 250.
 499

500 The terms $\Sigma(x_{EGM})^{-1}$ and $\Sigma(x_{EGM})^{-1}x_{EGM}$ denote the system of normal equations, which relies
 501 exclusively on the EGM2008 coefficients x_{EGM} up to degree/order 360, which are used as
 502 pseudo-observations (the Jacobian is in this case an identity matrix). Since for EGM2008 only
 503 the variances are available, the variance-covariance matrix $\Sigma(x_{EGM})^{-1}$ has a diagonal structure.
 504 The weight for the satellite-only system is $w_1 = 1$, expressing the fact that we consider the formal
 505 errors of this combined model as correctly scaled, and the weight of EGM2008 has been
 506 assigned empirically with $w_2 = 0.16$, and the EGM2008 formal errors have been down-scaled by
 507 a factor of 1 increasing linearly to 10 in range of degrees 180 to 200. In this way, the
 508 combination is tuned giving GRACE/GOCE data dominant influence in the degrees 0 to 180 and
 509 forcing EGM2008 information to take over in the spectral range 200 to 2190, leaving the main
 510 spectral range of transition from GRACE/GOCE to EGM2008, where both components
 511 contribute significantly, between degrees 180 to 200. Figure 2 shows the relative contributions of
 512 GOCE/GRACE data (red for more than 80% GOCE/GRACE impact) and indirectly the
 513 EGM2008 model contribution (blue for more than 80% EGM2008 impact) per spherical
 514 harmonic coefficient C_{nm} / S_{nm} in the combination (for degrees 0 to 250).

515



516
 517 Figure 2. Relative contribution of GOCE/GRACE data per spherical harmonic coefficient
 518 C_{nm} / S_{nm} in the combination with EGM2008 data (in percent) for the degrees 0 to 250

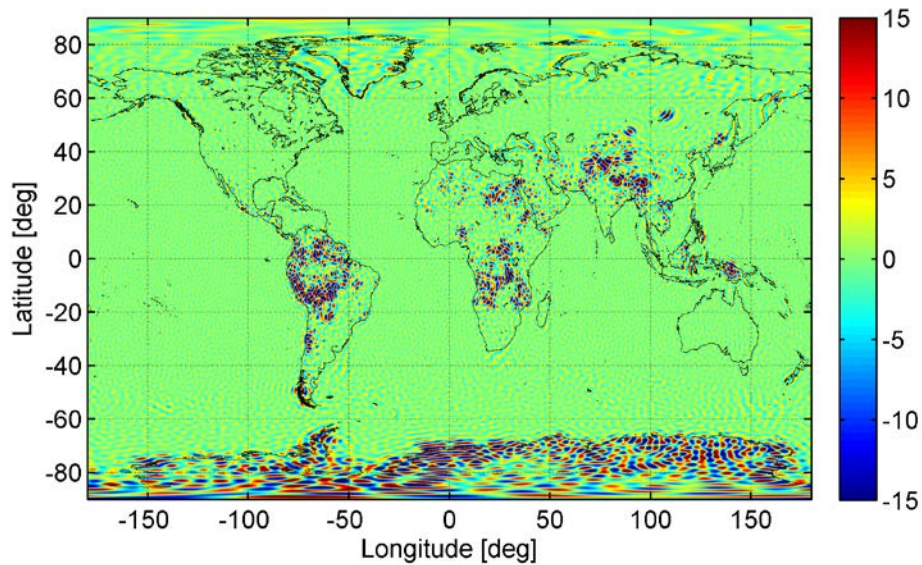
519
 520 From Fig. 2, the transition for certain harmonic orders (say $-20 < m < +20$) is differently than the
 521 other orders (say $m < -20, m > +20$). This is related to the lower accuracy for the determination of

522 the near-zonal spherical harmonic coefficients using GOCE gradiometry (known as the polar gap
523 problem due to the GOCE satellite's orbit inclination of 96.6 degrees). The lack of observations in
524 the polar regions worsens the accuracy in the determination of a certain group of spherical
525 harmonic coefficients, which is the near-zonal group (e.g., Sneeuw and Gelderen, 1997).
526 Consequently in the combined solution EGM2008 has a higher influence in for those coefficients
527 where GOCE shows a lower performance (and thus a higher standard deviation).

528

529 The outcome of this processing step is a combined GRACE/GOCE/EGM2008 coefficient data
530 set here denoted as GGE. Figure 3 shows the differences between gravity disturbances from
531 GGE and EGM2008, revealing significant discrepancies at the 10-20 mGal-level over Africa,
532 Asia and South America, while there is agreement in the mGal range over most parts of Europe,
533 Australia and North-America. The larger discrepancies are interpreted as improvements over
534 EGM2008 conferred by recent GRACE and GOCE data to GGMplus, see also *Pail et al.*, [2011]
535 and *Hirt et al.*, [2012].

536



537

538 Figure 3. Gravity disturbance differences between the GRACE/GOCE/EGM2008 merger GGE
539 and EGM2008-only in the spectral band of degrees 2 to 250, units in mGal

540

541 3.3 Synthesis

542

543 The spherical-harmonic coefficients (SHCs) of the combined GGE model were used in the
544 spectral band of degrees 2 to 2190 to synthesize gravity field functionals at the Earth's surface,
545 as represented through the 3D-coordinates (latitude, longitude, height). Accurate evaluation of
546 the SHCs requires taking into account the ellipsoidal height of the evaluation points which were
547 obtained from SRTM at 7.2 arc-second resolution. The zonal harmonics of the GRS80 normal
548 gravity field were subtracted from the GGE-model SHCs as described in *Smith* [1998]. The tide
549 system used in the synthesis is zero-tide, which is compatible with GRS80 [*Moritz*, 2000].

550

551 Spherical harmonic synthesis of gravity field functionals at the Earth's surface – known as 3D
552 synthesis – is computationally extraordinarily demanding, because efficient SHS operations

553 cannot be used [Holmes, 2003]. Therefore we used the gradient approach to higher order [Hirt,
 554 2012] which offers an efficient yet accurate approximate solution for 3D synthesis at densely-
 555 spaced surface points, represented through the elevation model. We used a modification of the
 556 harmonic_synth software [Holmes and Pavlis, 2008] to synthesize quasigeoid heights, gravity
 557 disturbances, North-South and East-West deflections of the vertical at a reference height of 4 km
 558 above the GRS80 reference ellipsoid at 1 arc-min resolution. For all four functionals radial
 559 derivatives were computed up to 5th-order at the same reference height and resolution. These
 560 were bicubically interpolated to 7.2 arc-second resolution and continued from the reference
 561 height to the Earth’s surface with 5th-order Taylor series expansions (cf. generic formulations
 562 provided in Hirt [2012]), yielding numerical estimates of gravity functionals at 3 billion surface
 563 points in the spectral band of degrees 2 to 2190.

564
 565 Using the gradient approach as described, the 3D synthesis of the four gravity field functionals
 566 took about 6 weeks of computation time using an in-house Sun Ultra 45 workstation. By
 567 comparison, 3D synthesis with conventional point-by-point evaluation methods [Holmes, 2003]
 568 would have taken an estimated 60 years of computation time. This estimate is based on an
 569 observed performance of 100 points/ minute using the same workstation and parameters. The 3D
 570 synthesis as applied here is therefore one of the key innovations that made the construction of
 571 GGMplus feasible within acceptable computation times.

572
 573 We note that the gradient approach is an approximate technique for 3D-SHS, whereby
 574 approximation errors decrease with increasing order of the Taylor series applied. From analysis
 575 of the 0th to 5th-order contributions over 3 billion points, the contribution made by subsequent
 576 orders (e.g., 0th and 1st, 1st and 2nd) differs by a factor of about 4 to 5 (see also Table 2). Given
 577 maximum contributions of 2 mm, 0.6 mGal and 0.1 arc-sec for the 5th-order, maximum
 578 approximation errors (due to truncation of the Taylor series after the 5th-order) will be generally
 579 smaller than 0.6 mm, 0.2 mGal and 0.03 arc-sec anywhere in our working area. Hence, the
 580 Taylor series as applied for GGMplus converge sufficiently, and approximation errors are
 581 negligible for practical applications.

582
 583 Table 2. RMS (root-mean-square) and maximum values of the 4th-order and 5th-order terms of
 584 the Taylor expansions used for gravity field continuation to the Earth’s surface. Also given are
 585 the estimated RMS and maximum approximation errors. Values reported for the functionals
 586 quasigeoid, gravity disturbances and deflections of the vertical.

Functional	Contribution of 4 th –order term		Contribution of 5 th –order term		Estimated approximation error	
	RMS	Max	RMS	Max	RMS	Max
Quasigeoid [mm]	0.24	9.88	0.05	2.07	0.01	0.52
Gravity [mGal]	0.06	2.54	0.01	0.59	0.00	0.15
NS deflection of the vertical [arc-sec]	0.01	0.31	0.00	0.08	0.00	0.02
EW deflection of the vertical [arc-sec]	0.01	0.34	0.00	0.08	0.00	0.02

587
 588 For quasigeoid heights, the C1B correction term [Rapp, 1997], see also [Hirt, 2012], was applied
 589 to take into account the change in normal gravity with height. For gravity disturbances, the

590 ellipsoidal correction was applied [Claessens, 2006]. For the North-South deflection of the
591 vertical, corrections for the curvature of the plumbline and for the ellipsoidal effect were taken
592 into account as described in [Jekeli, 1999].

593

594

595 3.4. Forward-modelling

596

597 Gravity forward-modelling based on high-resolution topography is a frequently-used technique
598 to derive information on the short-scale gravity field in approximation [Forsberg, 1984; Pavlis et
599 al., 2007; Hirt, 2012]. The short-scale (i.e., 10 km to ~250 m) gravity signals of the GGMplus
600 model are based on forward-modelling using the 7.5 arc-sec resolution (~250m) SRTM V4.1
601 topography [Jarvis et al., 2008] over land and the 30 arc-sec resolution SRTM30_PLUS V7.0
602 bathymetry [Becker et al., 2009] over sea. A small number of bad data areas (about 0.002% of
603 the total area covered by GGMplus as shown in Fig. 1) was identified and removed from both
604 data sets through simple hole-filling.

605

606 The forward-modelling approach applied here follows the description given in Hirt [2013]. In
607 brief, we converted the SRTM30_plus bathymetry to rock-equivalent depths before merging with
608 the 250m SRTM V4.1 topography. The merger was high-pass filtered by subtracting heights
609 from the RET2012 rock-equivalent topography model to degree and order 2160 (publicly
610 available from <http://geodesy.curtin.edu.au/research/models/Earth2012/>,
611 Earth2012.RET2012.SHCTo2160.dat).

612

613 We applied brute-force numerical integration techniques [Forsberg, 1984] to convert the high-
614 pass filtered topography (and rock-equivalent depths over sea) to topography-implied gravity,
615 geoid and vertical deflections. The forward-modelled gravity signals possess spectral energy at
616 spatial scales of ~10 km to ~250 m which augments GGE gravity information beyond 10 km
617 resolution. The numerical integration was accomplished with a variant of the TC software
618 [Forsberg, 1984] and an integration cap radius of 200 km around any of the ~3 billion
619 computation points, and the correction for Earth's curvature applied, as described in Forsberg
620 [1984]. Given the oscillating nature of the high-pass filtered topography, the effect of remote
621 masses largely cancels out as pointed out by Forsberg and Tscherning [1981]. The integration
622 radius chosen is suitable for forward-modelling of high-frequency gravity effects [Hirt et al.,
623 2010; Hirt, 2012].

624

625 The forward-modelling exercise was partitioned into ~19,000 computationally 'manageable'
626 areas of 1 deg x 1 deg extension covering land areas everywhere on Earth between $\pm 60^\circ$ -latitude
627 with SRTM data available. Each 1 deg x 1 deg tile is composed of 625,000 computation points at
628 7.2 arc-seconds resolution. We utilized the iVEC/Epic supercomputing facility
629 (<http://www.ivec.org/>) along with massive parallelization (simultaneous use of up to 1100 central
630 processing units (CPUs)) to accomplish the forward-modelling for the first time near-globally.
631 Based on non-parallelized standard computation techniques and a single CPU, the calculation of
632 topographic gravity effects had taken an estimated 20 years, which is why all previous efforts
633 were inevitably restricted to regional areas.

634

635 The topographic gravity effects calculations are based on the assumptions of constant mass-
636 density (standard rock density 2670 kg/m^3) and isostatically uncompensated topography, which
637 should well be justified given the spatial scales (less than 10 km) modelled here from
638 topographic information (e.g., *Torge*, [2001]; *Watts*, [2001]; *Wieczorek*, [2007]). Given that any
639 gravity field signals originating from mass-density variations [with respect to standard rock
640 density] are not represented by the topographic gravity, our GGMplus gravity maps cannot
641 provide geological information at scales less than 10 km. However, the same limitations apply to
642 EGM2008 at spatial scales less than ~ 27 km over many developing countries [*Pavlis et al.*,
643 2012] and to any other gravity field model with topographic information used to increase the
644 resolution among observed gravity.

645
646 Due to the chosen constant mass-density - often used as standard mass-density for gravity
647 reductions in geophysics and geodesy - the chosen value should approximates well the
648 topographically-induced gravitational attraction over granite rock (2700 kg m^{-3}), while the
649 approximation may introduce errors up to 7% over areas of volcanic rock (2900 kg m^{-3}), and
650 about ~ 26 % where sediments prevail (2000 kg m^{-3}). While inclusion of detailed mass-density
651 maps in the forward-modelling can reduce these errors, a detailed modelling of mass-density
652 variations was not attempted in this work because high-resolution density maps were not
653 available everywhere in our working area.

654
655 From comparisons with ground-truth data sets, a range of studies [e.g., *Hirt et al.*, 2010; *Hirt*,
656 2012; *Šprlák et al.*, 2012] demonstrate that short-scale topographic gravity effects are capable of
657 representing a significant portion (in some cases as high as 90 %) of real gravity field features
658 over rugged terrain, see also evaluation results in Section 5.

659 3.5 Calculation of normal gravity at the Earth's surface

660
661
662 For the construction of gravity acceleration maps, normal gravity (i.e., the gravitational attraction
663 and centrifugal acceleration generated by an oblate equipotential ellipsoid of revolution) was
664 calculated at the Earth's surface. We used the parameters of the GRS80 reference ellipsoid
665 [*Moritz*, 2000] along with the standard second-order Taylor expansion (*Torge* [2001], p 110, Eq.
666 4.63) to calculate normal gravity at the ellipsoidal heights of the Earth's surface, as represented
667 through the SRTM topography at 7.2 arc-sec spatial resolution. Beside the gravitational
668 attraction and centrifugal acceleration of the GRS80 mass-ellipsoid, the resulting normal gravity
669 values also contain the effect of gravity attenuation with height (free-air effect), because we
670 evaluated at the Earth's surface.

671 3.6 Combination of synthesis results, forward-modelling and normal gravity

672
673
674 All GGMplus gravity field functionals (quasigeoid heights, gravity disturbances, vertical
675 deflections) are the sum of

- 676 • Synthesized functionals from the GGE SHCs (providing the spatial scales of ~ 10000 km
677 down to ~ 10 km, Sect. 3.3) and
- 678 • Forward-modelled functionals from high-pass filtered topography/bathymetry data
679 (providing the spatial scales from ~ 10 km down to ~ 250 m, Sect. 3.4).

680 GGMplus gravity accelerations were obtained as the sum of GGMplus gravity disturbances and
 681 normal gravity values (Sect 3.5).

682

683 **4 Gravity estimation outside working area**

684

685 Due to Earth’s flattening, obvious candidate locations for Earth’s maximum gravity acceleration
 686 are expected near the poles, which is outside the $\pm 60^\circ$ -SRTM latitude band. To include a likely
 687 location for Earth’s maximum gravity acceleration in our work, we obtained gravity
 688 accelerations globally at 5-arc-min resolution without short-scale topographic gravity estimates,
 689 as follows:

- 690 1 We constructed a 5-arcmin grid of approximate ellipsoidal heights of the Earth’s surface
 691 as the sum of elevations from the Earth2012 Topo/Air model (representing Earth’s
 692 physical surface as lower interface of the atmosphere above mean sea level) and the
 693 EGM2008 quasigeoid applied as a correction.
- 694 2 We applied the gradient approach for harmonic synthesis (Sect. 3.3) to fifth-order,
 695 yielding gravity disturbances at the Earth’s surface in spectral band 2 to 2190 using the
 696 GGE coefficients (Sect 3.1).
- 697 3 We calculated normal gravity at the ellipsoidal heights of the Earth’s surface as described
 698 in Sect 3.5) and added the gravity disturbances, yielding gravity accelerations at 5 arc-
 699 min resolutions.

700 Steps 1 and 2 were applied to calculate a global 5 x 5 arc-min grid of quasigeoid heights which
 701 was then used to locate where the quasigeoid is likely to be furthest below the ellipsoid. The
 702 locations of the minimum and maximum gravity accelerations and quasigeoid heights are
 703 reported in Tables S3 and S4.

704

705 Table 3. Extreme values of gravity accelerations estimated based on 5 arc-min resolution

Extreme value	Latitude	Longitude	Value [mGal]	Comment
Minimum gravity acceleration	-9.88	-77.21	976790	GGMplus suggests a smaller value at a nearby location.
Maximum gravity acceleration	86.71	61.29	983366	Located offshore in the Arctic sea, not covered by GGMplus. Location and value reported in Table 1 in the main paper.

706

707 Table 4. Extreme values of quasigeoid heights estimated based on 5 arc-min resolution

Extreme value	Latitude	Longitude	Value [m]	Comment
Minimum quasigeoid height	4.71	78.79	-106.59	Located offshore (Laccadive Sea, South of Sri Lanka), not covered by GGMplus. Location and value reported in Table 1 in the main paper.
Maximum quasigeoid height	-4.21	138.71	86.48	GGMplus suggests a larger value at another location.

708

5. Model evaluation

We have evaluated GGMplus gravity field functionals using (i) gravity accelerations from terrestrial gravimetry, (ii) deflections of the vertical from geodetic-astronomical observations, and (iii) observed quasigeoid heights from GPS ellipsoidal heights and geodetic levelling (GPS/levelling). The data sets used are summarized in Table 5. Each set of observations is compared against the three modelling variants

- satellite-only gravity (GRACE combined with 4th-GOCE release) to degree and order 200 (resolution of ~100 km)
- satellite gravity combined with EGM2008 (GGE), to degree 2190 (resolution of ~10 km)
- GGMplus (resolution of ~200 m)

The descriptive statistics of the differences “observation minus model” are reported in Tables 6 and 7 for gravity disturbances, in Table 8 for deflections of the vertical and in Table 9 for quasigeoid heights. From the comparisons over North America, Europe and Australia – areas with good ground gravity coverage – the accuracy of GGMplus is at the 3-5 mGal, 1 arc-sec and 5-7 cm level or somewhat better for gravity, deflections of the vertical and quasigeoid heights, respectively. The RMS-improvements conferred by the short-scale gravity modelling (compare GGMplus with GGE) range between ~20 to ~90 % for the radial (gravity) and horizontal field components (deflections of the vertical), and is lower (non-significant to ~40% over Switzerland as an example of a mountainous region) for quasigeoid heights. Fig. 4 exemplifies the good agreement between observed gravity and GGMplus over Australia. The differences mostly reflect the effect of local mass-density variations, and can be used for geophysical interpretation. Fig. 4 also shows oscillations of 1-2 mGal amplitude and ~200 km full-wavelength which are likely to reflect the error level of GOCE satellite observations used in GGMplus.

Over less well-surveyed areas, the differences increase to ~8 to ~23 mGal, as is indicated by the few ground gravity observations available. Given that the forward-modelling of gravity effects at spatial scales of ~10 km to 200 m is based on a homogeneous procedure everywhere between ± 60° geographic latitude, there is no reason to assume a reduced performance over Asia, Africa and South America. The deterioration rather reflects the limited data availability for EGM2008 at spatial scales of ~100 to 10 km. The accuracy of GGMplus gravity field functionals is therefore largely dependent on the EGM2008 model commission errors, which can be as high as ~30-35 cm for quasigeoid heights, and ~4 arc-seconds for deflections of the vertical [Pavlis *et al.*, 2012]. We therefore expect the GGMplus accuracy to deteriorate by factor 3-5 from well-surveyed to poorly-surveyed continents.

Table 5. Gravity field observations used for evaluation of GGMplus.

Observation type	Country/ Area	# Stations	Data source/provider
Gravity accelerations and disturbances from terrestrial	United States	1,277,637	University of Texas at el Paso http://research.utep.edu/default.aspx?tabid=37229 2012 release
	Australia	1,625,018	Geoscience Australia

gravimetry			http://www.geoscience.gov.au 2013 release
	Switzerland	31,598	Swisstopo, Dr U Marti
	Central Africa	41,148	Bureau Gravimétrique International, Dr S Bonvalot
	India/Himalayas	7,562	Bureau Gravimétrique International, Dr S Bonvalot
	Northern South-America	12,150	Bureau Gravimétrique International, Dr S Bonvalot
Deflections of the vertical from geodetic- astronomical observations	United States	3,396	National Geodetic Survey, Drs D Smith and Y Wang
	Australia	1,063	Geoscience Australia/ Dr W Featherstone (Curtin University)
	Europe	1,056	ETZ Zurich, Dr B Bürki; Swisstopo, Dr U Marti; first author's own observations
GPS/levelling/ quasigeoid heights	United States	18972	National Geodetic Survey, http://www.ngs.noaa.gov/NGSDDataExplorer/
	Germany	675	Bundesamt für Kartographie und Geodäsie, U Schirmer
	Switzerland	193	Swisstopo, Dr U Marti

748

749

Table 6. Descriptive statistics of the differences observed gravity minus models, units in mGal

Terrestrial data	Model	Min	Max	Mean	RMS
US gravity	Satellite-only	-238.85	204.19	6.83	27.41
	GGE	-271.88	110.10	-2.70	10.80
	GGMplus	-303.39	88.84	-0.68	3.49
Australian gravity	Satellite-only	-179.98	118.24	-1.14	14.88
	GGE	-194.33	82.65	-1.07	5.03
	GGMplus	-193.15	81.06	-0.71	2.90
Swiss gravity	Satellite-only	-235.04	131.13	-35.49	67.21
	GGE	-226.64	93.38	-17.59	39.72
	GGMplus	-91.23	28.71	-0.60	4.41

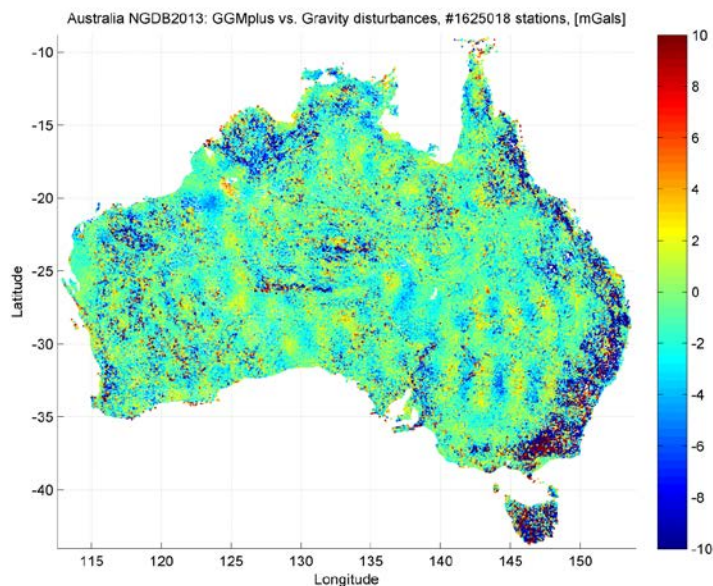
750

751

Table 7. Descriptive statistics of the differences observed gravity minus models, units in mGal

Terrestrial data	Model	Min	Max	Mean	RMS
Central Africa	Satellite-only	228.79	394.56	- 1.33	26.91
	GGE	-275.02	403.27	-0.15	9.68
	GGMplus	-284.41	399.87	0.37	8.24
India+ Himalayas	Satellite-only	-329.51	365.47	-5.23	43.53
	GGE	-184.46	341.92	0.04	21.84
	GGMplus	-182.44	309.74	2.45	13.76
Northern South- America	Satellite-only	-247.71	365.75	-11.66	66.52
	GGE	-224.32	361.48	-4.60	26.18
	GGMplus	-234.27	364.00	-0.03	22.69

752



754
755 Figure 4. Differences between observed gravity accelerations and GGMplus over Australia, units
756 in mGal.

757
758 Table 8. Descriptive statistics of the differences observed deflection of the vertical (DoV) minus
759 models, units in arc-seconds

Terrestrial data	Model	Min	Max	Mean	RMS
US North-South DoVs	Satellite-only	-19.59	22.62	0.20	3.27
	GGE	-12.55	21.29	0.09	1.11
	GGMplus	-12.58	20.97	-0.02	0.84
US East-West DoVs	Satellite-only	-22.66	23.41	0.29	3.78
	GGE	-13.57	12.38	0.10	1.14
	GGMplus	-6.19	9.90	0.12	0.78
Australian North-South DoVs	Satellite-only	-11.58	11.76	-0.14	2.21
	GGE	-5.00	3.44	-0.23	0.81
	GGMplus	-5.13	2.61	-0.19	0.66
Australian East-West DoVs	Satellite-only	-18.01	11.68	-0.14	2.63
	GGE	-4.87	3.60	-0.11	1.04
	GGMplus	-5.05	4.05	-0.13	0.97
Europe North-South DoVs	Satellite-only	-19.49	26.96	0.88	6.41
	GGE	-15.06	15.62	0.05	3.02
	GGMplus	-4.86	5.51	-0.05	1.06
Europe East-West DoVs	Satellite-only	-24.05	24.97	0.90	5.87
	GGE	-11.58	15.65	0.38	2.98
	GGMplus	-4.29	4.99	0.23	1.09

764 Table 9. Descriptive statistics of the differences observed quasigeoid height minus models, units
 765 in m. In case of US GPS/levelling data, observed geoid heights were converted to quasigeoid
 766 heights applying Rapp's (1997) formalism [1] prior to comparison with the three modelling
 767 variants. A bias (Germany, Switzerland), and tilted plane (US) were subtracted.

Terrestrial data	Model	Min	Max	RMS
US GPS/lev	Satellite-only	1.80	2.72	0.367
	GGE	-0.34	0.42	0.070
	GGMplus	-0.36	0.43	0.070
German GPS/lev	Satellite-only	-1.07	1.42	0.315
	GGE	-0.11	0.17	0.042
	GGMplus	-0.10	0.14	0.041
Swiss GPS/lev	Satellite-only	-1.27	1.86	0.605
	GGE	-0.24	0.18	0.076
	GGMplus	-0.17	0.13	0.046

768

769 Additional References

770

771 Becker, J.J., D.T. Sandwell, W.H.F. Smith, J. Braud, B. Binder, J. Depner, D. Fabre, J. Factor, S. Ingalls,
 772 S-H. Kim, R. Ladner, K. Marks, S. Nelson, A. Pharaoh, R. Trimmer, J. Von Rosenberg, G. Wallace
 773 and P. Weatherall (2009), Global Bathymetry and Elevation Data at 30 Arc Seconds Resolution:
 774 SRTM30_PLUS, *Marine Geod.*, 32(4), 355-371.

775 Claessens, S.J., (2006), Solutions to Ellipsoidal Boundary Value Problems for Gravity Field Modelling,
 776 PhD thesis, Department of Spatial Sciences, Curtin University of Technology, Perth, Australia.

777 Claessens, S.J., W.E. Featherstone, I.M. Anjasmara, and M.S. Filmer (2009), Is Australian data really
 778 validating EGM2008 or is EGM2008 just in/validating Australian data, in *Newton's Bulletin* 4, 207-
 779 251, Publication of the International Association of Geodesy and International Gravity Field
 780 Service.

781 Forsberg, R. (1984), A study of terrain reductions, density anomalies and geophysical inversion methods
 782 in gravity field modelling, Report 355, *Department of Geodetic Science and Surveying*, Ohio State
 783 University, Columbus.

784 Hirt, C. (2012), Efficient and accurate high-degree spherical harmonic synthesis of gravity field
 785 functionals at the Earth's surface using the gradient approach, *J. Geod.*, 86(9), 729-744, doi:
 786 10.1007/s00190-012-0550-y.

787 Hirt, C. (2013), RTM gravity forward-modeling using topography/bathymetry data to improve high-
 788 degree global geopotential models in the coastal zone, *Marine Geod.*, 36(2):1-20,
 789 doi:10.1080/01490419.2013.779334.

790 Hirt C., M. Kuhn, W.E. Featherstone, and F. Goettl (2012), Topographic/isostatic evaluation of new-
 791 generation GOCE gravity field models. *J. Geophys. Res.* B05407.

792 Holmes, S.A., (2003), High degree spherical harmonic synthesis for simulated earth gravity modelling,
 793 PhD Thesis, Department of Spatial Sciences, Curtin University of Technology, Perth, Australia.

794 Holmes S.A., and N.K. Pavlis (2008), Spherical harmonic synthesis software harmonic_synth.
 795 http://earth-info.nga.mil/GandG/wgs84/gravitymod/new_egm/new_egm.html.

796 Jarvis, A., H.I. Reuter, A. Nelson, and E. Guevara. (2008). Hole-filled SRTM for the globe Version 4,
 797 Available from the CGIAR-SXI SRTM 90m database. Available at: <http://srtm.csi.cgiar.org>.

798 Jekeli C (1999), An analysis of vertical deflections derived from high-degree spherical harmonic models.
 799 *J. Geod.* 73(1), 10-22.

800 Mayer-Gürr, T., E. Kurtenbach, and A. Eicker (2010), ITG-Grace2010 Gravity Field Model. URL:
 801 <http://www.igg.uni-bonn.de/apmg/index.php?id=itg-grace2010>, 2010.

802 Moritz, H. (2000), Geodetic Reference System 1980. *J. Geod.*, 74, 128-140.

803 Pail R., T. Fecher, M. Murböck M. Rexer, M. Stetter, T. Gruber, and C. Stummer, (2013), Impact of
804 GOCE Level 1b data reprocessing on GOCE-only and combined gravity field models. *Stud.*
805 *Geophy. Geod.* 57, 155-173.

806 Pavlis, N.K., J.K. Factor, and S.A. Holmes (2007), Terrain-related gravimetric quantities computed for
807 the next EGM, in *Proceedings of the 1st International Symposium of the International Gravity Field*
808 *Service* 318-323, Harita Dergersi, Istanbul.

809 Pavlis N.K., S.A. Holmes, S.C. Kenyon, and J.K. Factor (2012), The development and evaluation of the
810 Earth Gravitational Model 2008 (EGM2008), *J. Geophys. Res.*, 117, B04406,
811 doi:10.1029/2011JB008916.

812 Rapp R.H (1997), Use of potential coefficient models for geoid undulation determinations using a
813 spherical harmonic representation of the height anomaly/geoid undulation difference, *J. Geod.* 71(5),
814 282-289.

815 Smith, D.A. (1998), There is no such thing as "The" EGM96 geoid: Subtle points on the use of a global
816 geopotential model, in *International Geoid Service Bulletin* 8, 17-28, International Geoid Service,
817 Milan, Italy.

818 Sneeuw N., van Gelderen, M. (1997), The polar gap. In: *Geodetic boundary value problems in view of the*
819 *one centimeter geoid. Lecture notes in Earth Sciences*, 65, 559–568, Springer, Berlin,
820 doi:10.1007/BFb0011699

821 Šprlák, M., C. Gerlach, and B.R. Pettersen, (2012), Validation of GOCE global gravity field models using
822 terrestrial gravity data in Norway. *J. Geod. Sci.* 2, 134-143.

823 Stummer C., T. Fecher, and R. Pail (2013), Alternative method for angular rate determination within the
824 GOCE gradiometer processing. *J. Geod.* 85, 585-596 (2011).

825 Torge, W. (2001), *Geodesy, 3rd Edition.*, De Gruyter, Berlin, New York.

826 Watts, A.B. (2001), *Isostasy and Flexure of the Lithosphere.* Cambridge University Press.

827 Wieczorek M.A. (2007), Gravity and topography of the terrestrial planets, in *Treatise on Geophysics* 10,
828 165, Elsevier-Pergamon, Oxford.

829